JOURNAL OF SPACECRAFT AND ROCKETS
Vol. 34, No. 6, November–December 1997

Methods for Distributing Semiempirical, Nonlinear, Aerodynamic Loads on Missile Components

F. G. Moore* and R. M. McInville†
U.S. Naval Surface Warfare Center, Dahlgren, Virginia 22448-5100
and
Clint Housh‡
U.S. Naval Air Warfare Center, China Lake, California 93555-6001

New methodology has been added to the U.S. Naval Surface Warfare Center, Dahlgren Division, Aeroprediction code to permit the distribution of the local linear and nonlinear aerodynamic loads along the body length and over the wing and tail lifting surfaces. The new techniques extend to both the Φ = 0 and 45 deg roll positions and to both windward and leeward lifting surfaces in the 45-deg roll orientation. The local loads are integrated to get the distribution of the shear and bending moments for use in structural analysis and design. Navier–Stokes computational fluid dynamics computations for a wing–body–tail missile configuration were used in the development of these extensions of the code and in validating their effectiveness. In general, good agreement with total force and moment experimental data and the computational fluid dynamics results is obtained.

Nomenclature

A_{ref} = reference area (maximum cross-sectional area of body, if a body is present, or planform area of wing if wing alone), ft^2
$BM(x)_B$ = body bending moment as a function of streamwise coordinate, lb-ft
$BM(y)_{W/T}$ = wing or tail bending moment as a function of spanwise coordinate, lb-ft
b_T, b_W = tail or wing span not including body, ft
C_N = total normal force coefficient
C_{N_B} = normal force coefficient of the body
$C_{N_{T(B)}}, C_{N_{W(B)}}$ = normal force coefficient of tail or wing in presence of body
$C_{N_{T(V)}}$ = component of normal force coefficient in tail region due to interference from wing
$[C_{N_{T(V)}}]_{\text{body,tail}}$ = portion of total wing–tail interference term assigned to body or tail
$[C_{N_{T(V)}}]_{\text{leeward,windward}}$ = portion of tail component of wing–tail interference term assigned to the leeward or windward tail surfaces
$(C_{N_\alpha})_W$ = change of wing normal force coefficient with angle of attack, rad^{-1}
$(C_r)_{T,W}$ = root chord of tail or wing lifting surface, ft
$c(y)_T, c(y)_W$ = local chord of tail or wing as a function of spanwise coordinate, ft
$\{[c_n(y)]_L\}_{T,W}$ = linear component of local normal force coefficient on tail or wing as a function of spanwise coordinate
$[c_n(y)]_{\text{leeward,windward}}$ = portion of total local normal force coefficient assigned to the leeward or windward lifting surfaces
$[c_n(y)]_{T,W}$ = local normal force coefficient on tail or wing as a function of spanwise-coordinate
$[c_n(y)]_{T(V)}$ = portion of local normal force coefficient on lifting surfaces attributed to wing–tail interference
$c_{n_B}, (c_{n_B})_L, (c_{n_B})_{NL}$ = local total, linear, and nonlinear normal force coefficient of the body
$(c_{n_B})_{NL,\text{adj}}$ = nonlinear component of body local normal force coefficient adjusted for decreased nose loads
$(c_{n_B})_{T(V)}$ = component of body local normal force coefficient due to wing–tail interference
D_B = diameter of body, ft
i_1, i_4 = interference factors in wing–tail interference calculations for windward and leeward plane wings, respectively
$K_{B(W)}$ = ratio of additional body normal force coefficient in the presence of a wing to that of the wing alone where δ is 0 deg
$\{[K_{B(W)}]_{\min}\}_{\Phi=0,45}$ = minimum value of $K_{B(W)}$ where Φ is at 0- or 45-deg roll position
$K_{W(B)}$ = ratio of lifting surface normal force coefficient in the presence of a body to that of the lifting surface alone where δ is 0 deg
$k_{W(B)}$ = ratio of normal force contribution of a deflected lifting surface in the presence of a body to that of the lifting surface alone where α is 0 deg
M = Mach number
Q = dynamic pressure, lb/ft^2
r = local body radius, ft
r_{vort} = vortex radius, ft
$VC(y)$ = vortex strength–local chord parameter
$V(x)_B$ = body shear as a function of streamwise coordinate, lb
$V(y)_{W/T}$ = wing or tail shear as a function of spanwise coordinate, lb
$w(x)_B$ = local body load as a function of streamwise coordinate, lb/ft
$w(y)_T$ = local tail load as a function of spanwise coordinate, lb/ft
$w(y)_W$ = local wing load as a function of spanwise coordinate, lb/ft
x = streamwise coordinate, ft
y = spanwise lifting surface coordinate, ft
y_{dist} = spanwise distance from path of vortex shed from wing to local point on tail, ft

Received Sept. 5, 1996; revision received May 15, 1997; accepted for publication May 15, 1997.

*Senior Aerodynamicist, Dahlgren Division, Weapons Systems Department. Associate Fellow AIAA.
†Aerospace Engineer, Dahlgren Division, Aeromechanics Branch, Weapons Systems Department.
‡Aerospace Engineer, Weapons Division, Airframe, Ordnance, and Propulsion Branch.

y_{vort} = spanwise distance from centerline of body to path of vortex shed from wing
α = angle of attack, rad, deg
$\Delta C_{N_{B(T)}}, \Delta C_{N_{B(W)}}$ = increment to normal force coefficient on body due to presence of tail or wing
$\Delta c_{n_{B(W)}}, \Delta c_{n_{B(T)}}$ = local normal force coefficient load induced on the body due to presence of wing or tail, respectively
δ = deflection angle of control surface, rad, deg
Φ = roll position of missile, when equal to 0 deg, corresponds to fins in the plus orientation

Introduction

THE Naval Surface Warfare Center, Dahlgren Division, Aeroprediction code (AP95) (Ref. 1) allows the computation of aerodynamics over an extensive range of flight conditions that includes the operating environments encountered by most tactical missiles. This range covers angles of attack (AOA) up to 90 deg, Mach numbers from 0 to 15, and control deflections from −30 to +30 deg. Originally, it was limited to the roll position of $\Phi = 0$ deg [fins in the plus (+) position], but Ref. 2 recently extended the code to the $\Phi = 45$ deg [fins in the cross (×) position] roll orientation.

The latest public release of the AP95 code incorporates the capability to model nonlinear aerodynamic loads. These nonlinear loads are estimated in an approximate analytical or semiempirical sense by separating each aerodynamic force component into a linear and nonlinear term. As in previous versions of the code, the linear term is modeled by the application of either linear, slender body, or second-order theory. The resulting pressure distributions can be integrated to produce aerodynamic loading information for use in structural design and analysis. The nonlinear contribution, however, is modeled by the direct application of wind-tunnel data-bases and is defined primarily in terms of total force and moment information. Some distribution information is provided for the nonlinear component of the body loads, but none is currently available for the lifting surface loads or for their interference effects on the body. This situation is not restrictive in terms of aerodynamic and performance analysis. Structural engineers, however, need to know not only the magnitude of the aerodynamic forces, but also how they are spread over the surface of a missile if they are to determine the shear and bending moments to which its components will be subjected. For this reason, the AP95 code is being modified to allow the prediction of the distribution of the nonlinear, as well as the linear, aerodynamic loads over both the body and control surfaces. All interference effects will be included in the analysis, in addition to the individual component nonlinear aerodynamics. This new technology, along with several recent and current improvements to the AP95 will be transitioned to users in 1998 as the AP98. The approach taken to distribute these nonlinear loads is the subject of this paper.

Analysis

The overall approach to model the nonlinear load distribution for the AP98 was the following.

1) Pick a missile configuration that has two sets of lifting surfaces and a good set of force and moment wind-tunnel data over a fairly broad range of freestream conditions. The configuration chosen is shown in Fig. 1, and the wind-tunnel data set is given in Ref. 3.

2) Use a Navier–Stokes (NS) solver and refine the mesh until the total force and moment results do not change to an appreciable extent. The code selected was the thin layer NS code referred to as Overflow.[4]

3) Compare the computational fluid dynamics (CFD) predicted force and moment and center of pressure data to the experimental data of Ref. 3. If the comparisons agree reasonably well over a broad range of conditions, we will assume that the code is accounting for all of the physics reasonably well and that the local loads on the body and lifting surfaces are also correct.

4) Derive methods for distributing the nonlinear component of the aerodynamic loads over the body and lifting surfaces for use in the AP98.

Table 1 Comparison of CFD calculations[5] to experiment[3]

Mach number	AOA, α	Roll, Φ	CL, % difference, exp. vs CFD	CD, % difference, exp. vs CFD	X_{CP} difference, % body length, exp. vs CFD
1.50	10	0	1.8	6.1	0.78
1.50	25	0	1.1	2.6	0.57
1.50	40	0	−0.7	0.4	0.07
2.87	10	0	2.1	5.9	1.44
2.87	25	0	−1.5	−0.7	0.07
2.87	40	0	−1.4	−2.9	0.38
4.60	10	0	0	−8.3	1.13
4.60	25	0	1.2	4.3	0.35
4.60	40	0	−6.1	−7.4	2.42
1.50	10	45	2.4	15.0	0.85
1.50	25	45	0.4	0.6	0.44
1.50	40	45	−1.5	−0.7	−0.09
2.87	10	45	−1.6	12.1	1.22
2.87	25	45	−3.0	3.1	0.77
2.87	40	45	−0.9	−0.8	0.56
4.60	10	45	−5.6	6.7	1.58
4.60	25	45	−0.6	3.6	1.21
4.60	40	45	0.5	1.8	0.82

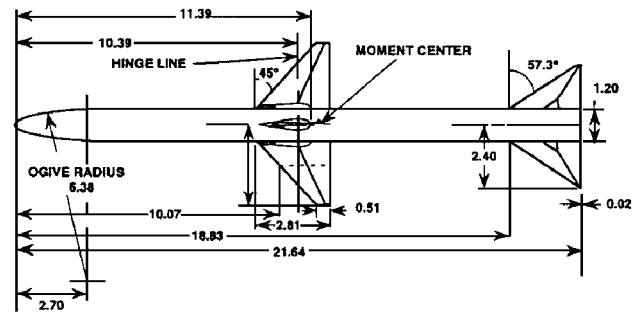

Fig. 1 Wing–body–tail missile configuration.

Table 1 presents the results of the CFD calculations compared to experiment (the reader is referred to Ref. 5 for the detailed discussion of the NS computations and theory discussed in this article). The errors in Table 1 are defined as the difference between experiment and CFD results divided by the experimental results. As seen in Table 1, the comparisons are quite good with a couple of exceptions. These are at low AOA ($\alpha = 10$ deg), where the error in reading the data points from the graph can be a significant portion of the data, and at the case for $\alpha = 40$ deg, $\Phi = 0$ deg, and $M = 4.6$. This case shows the CFD results to be off by 6–7% on both lift and drag and center of pressure by over 2% of body length. It is suspected that the strong internal shock interactions that occur at this AOA and Mach number require a full NS solution vs a thin-layer code to account for the streamwise and circumferential gradients of the stress terms. The other possibility is that a finer grid is needed than that used for this case.

Overall, the results of Table 1 were considered quite acceptable for use in deciding how to distribute the nonlinear aerodynamic loads in the aeroprediction code. The average accuracy levels of the lift coefficient was better than 2% and the center of pressure about 1% of the body length. These are the main force and moment contributors to local loads, shear, and bending moment for use in structural analysis. The remainder of the analysis portion of this paper will discuss the approach of how each nonlinear aerodynamic component is treated to accomplish the task of distributing these loads in a semiempirical code. The total normal force for a wing–body–tail configuration can be defined by

$$C_N = C_{N_B} + C_{N_{W(B)}} + \Delta C_{N_{B(W)}} + C_{N_{T(B)}} + \Delta C_{N_{B(T)}} + C_{N_{T(V)}} \quad (1)$$

The first term in Eq. (1) is the normal force coefficient of the body, alone. The second term is the normal force coefficient of the wing in the presence of the body, and the third represents the additional component of normal force on the body due to the presence of the wing. The fourth term is the normal force coefficient of the tail in

the presence of the body, and the fifth represents the incremental normal force on the body as a result of the tail. The final term is the normal force on the tail, usually negative, caused by the vortices shed from the wing.

Each of the terms in Eq. (1) has a linear and a nonlinear component. Either linear theory or slender body theory is used to determine the linear portion of each term, and the nonlinear contributions are computed directly from wind-tunnel databases, with engineering judgment and extrapolation being used where database information is limited. Overall average accuracy is maintained at ±10% for the total normal and axial force coefficients and ±4% of total body length for the center of pressure.

In the following sections, each component of Eq. (1) will be considered individually, and the methodology that has been developed to distribute its nonlinear elements over the body surface will be briefly discussed. First, the $\Phi = 0$ deg roll position will be addressed, and then any changes or additions that are necessary to extend the methodology to the $\Phi = 45$ deg roll position will be presented. Those interested in the details of the theoretical discussions are once again referred to Ref. 5.

Body Loads at the $\Phi = 0$ deg Roll Position

Four of the terms in Eq. (1) contribute to the body loading. These are C_{N_B}, $\Delta C_{N_{B(W)}}$, $\Delta C_{N_{B(T)}}$, and $C_{N_{T(V)}}$. The first three of these will be discussed directly following this section. The wing–tail interference will be reserved for the section following lifting surface loads inasmuch as it is connected directly to them and is shared with the tail surfaces.

Body-Alone Loads

The body-alone component C_{N_B} is composed of a linear and a nonlinear load. The linear load is computed analytically above $M = 1.2$ by either Van Dyke's hybrid theory combined with modified Newtonian theory[6] or second-order shock-expansion theory.[7] Pressure coefficients are computed as a function of position along and around the body and then integrated along the body to obtain local linear normal force.

The nonlinear body normal force coefficient contribution is computed by a modification of the Allen–Perkins viscous crossflow theory[1,2] and distributed uniformly along the body surface. The total local normal force coefficient at any point along the body surface is the sum of the linear and nonlinear components. That is,

$$c_{n_B} = \left(c_{n_B}\right)_L + \left(c_{n_B}\right)_{NL} \tag{2}$$

Comparison of Eq. (2) with results from CFD computations[5] indicated that the predicted body load in the nose region was too high at low AOA. It is believed that this discrepancy occurs because, at low AOA, the point at which the body vortices begin to separate is toward the afterbody of the missile. Then, as AOA is increased, the separation point moves forward and the full effect of the body shed vortices is apparent. To account for this effect, the nonlinear load contribution of Eq. (2) was adjusted at low AOA.

On the nose itself, the nonlinear load is reduced at AOA below $\alpha = 30$ deg by a factor that varies linearly with AOA from 1 at $\alpha = 30$ deg to 0 at $\alpha = 0$ deg. No adjustment is made at AOA above 30 deg. There is a transition region, which extends for a distance of two calibers from the end of the nose, within which the nonlinear load component is allowed to recover gradually from its reduced value at the end of the nose to its normally computed level at that location. Because the total normal force computed by AP95 agrees well with experimental results, the portion of the nonlinear loads that are removed from the nose and transition regions must be added back into the loads on the remainder of the body. Thus, for points on the body more than two calibers downstream of the nose, the normally computed local nonlinear loads are increased by terms that represent the total load reductions in the nose and transition regions, respectively, spread evenly over the total remaining body length.

Body–Wing and Body–Tail Interference Loads

For the discussion to follow, forward lifting surfaces will be referred to as wings, and aft lifting surfaces will be referred to as the tail. In the vicinity of any lifting surface, the body is subjected to increased loads caused by interference effects. These contributions, represented in Eq. (1) by $\Delta C_{N_{B(W)}}$ for the wing and by $\Delta C_{N_{B(T)}}$ for the tail, are also computed as separate linear and nonlinear components with afterbody effects being considered for the rear lifting surfaces. Therefore, the region of influence of the lifting surfaces on the body is consistent with the method currently used for moment and center of pressure calculations in the AP95. This method basically assumes the region of carryover lift onto the body is based on the region influenced by the local Mach lines from the wings or tails as they sweep across the body surface. The region of load on the body consists of a trapezoidal shape with total height defined by the magnitude of the aerodynamic interference terms, $\Delta C_{N_{B(W)}}$ and $\Delta C_{N_{B(T)}}$, the Mach number, body diameter, and root chord lengths of the wing or tail.[5]

In situations where the wing or tail is located near the aft end of the body, it is possible for the Mach lines to extend beyond the body, and some of the interference loading will be lost unless further adjustments are made. For these cases, the cross-sectional area of the body enclosed by the Mach lines and the aft end of the body is determined and compared to the total cross-sectional area that would be enclosed by the Mach lines if the body were not cut off. The maximum interference load values are then adjusted to compensate for the lost area and maintain the correct total of interference normal force as computed by the AP95.

Lifting Surface Loads at the $\Phi = 0$ deg Roll Position

The total contributions to the normal force of the wing and tail are represented in Eq. (1) by $C_{N_{W(B)}}$ and $C_{N_{T(B)}}$, respectively. Using $C_{N_{W(B)}}$ as an example, these two terms each have the following form:

$$C_{N_{W(B)}} = \left[K_{W(B)} \sin\alpha + k_{W(B)} \sin\delta\right]\left(C_{N_\alpha}\right)_W \tag{3}$$

Nonlinearities are introduced into $C_{N_{W(B)}}$ by defining both a linear and a nonlinear contribution for the normal force of the isolated wing, represented by $(C_{N_\alpha})_W$, and for each of the interference factors $K_{W(B)}$ and $k_{W(B)}$, which are introduced to account for the effects of the presence of a body on the normal force of the lifting surface.

The linear part of the local normal force coefficient on a wing or tail surface at a spanwise location y is computed by either lifting surface theory for subsonic flows or three-dimensional thin wing theory for supersonic flows.

The nonlinear part of the wing-alone lift is determined using a fourth-order analytical method[8] in conjunction with wing-alone databases.[9–11] Only the total values of lift and moment are available from the databases with no surface distribution information included. This distribution will be determined in conjunction with that of the interference factors.

From the combined linear and nonlinear wing-alone normal force, C_{N_α} is determined based on a secant slope of the total AOA, $|\alpha + \delta|$, experienced by the lifting surface. This slope is then multiplied by $\sin\alpha$ and $\sin\delta$ terms, which contain the interference factors $K_{W(B)}$ and $k_{W(B)}$, respectively, to account for the interference effects of the body on the wing. (All subscripts have been dropped from K and k for simplicity.) The linear contributions to $K_{W(B)}$ and $k_{W(B)}$ are found from slender body theory. These linear values are then adjusted for nonlinear[9–11] effects based on information from wind-tunnel databases. As for the wing-alone case, these databases provide only total force and moment measurements and, therefore, a method must be developed to distribute the nonlinear component of $K_{W(B)}$ and $k_{W(B)}$ along the span.

As mentioned already, the AP95 code computes the spanwise distribution of the linear normal force of an isolated lifting surface. It will be assumed that the nonlinear contributions to the wing-alone normal force and the interference effects, represented by the $K_{W(B)}$ and $k_{W(B)}$ factors, will be distributed in the same manner. Thus, at any y location, the local load $c_n(y)$ for the wing and tail will be

$$[c_n(y)]_W = \{[c_n(y)]_L|\}_W \left(\frac{C_{N_{W(B)}}}{\sum_{\text{span}}\{[c_n(y)]_L\}_W}\right) \tag{4}$$

and

$$[c_n(y)]_T = \{[c_n(y)]_L\}_T \left(\frac{C_{N_{T(B)}}}{\sum_{\text{span}} \{[c_n(y)]_L\}_T} \right) \tag{5}$$

Wing–Tail Interference

The AP95 code computes only the total value of the wing–tail interference term [$c_{N_{T(V)}}$ in Eq. (1)]. In this instance, however, not only is a method of spanwise distribution on the tail needed, but it is also apparent that a portion of the downwash effects should be carried over to the body. The division of $C_{N_{T(V)}}$ between the tail and body will be considered first. The method in which this objective is accomplished is not rigorous, but does have some intuitive foundation and is probably as well as can be done with the limited amount of CFD data available.

The assumption is made, from slender body theory, that the vortices from the forward lifting surfaces are shed from a spanwise location y_{vort} of

$$y_{\text{vort}} = (\pi/4)(b_W/2) + (D_B/2) \tag{6}$$

and travel straight back parallel to the velocity vector from this point. A relative value for the effect of this shed vortex on the tail surface at any chordwise point is given by

$$VC(y) = \left(\frac{1}{r_{\text{vort}} + y_{\text{dist}}} \right)^2 c(y)_T \tag{7}$$

where

$$y_{\text{dist}} = |y_{\text{vort}} - y| \tag{8}$$

and r_{vort} is a vortex radius taken to be 0.04. This value of r_{vort} could be subject to adjustment in the future as additional CFD or experimental data become available. An inspection of Eq. (7) shows that, at any point y, it consists of the product of a factor that is proportional to the local vortex strength through the inverse square distance term and a second factor, represented by the local chord, that is related to the local area affected by the vortex. The use of an absolute value for y_{dist} assures that the relation will be valid regardless of where the vortex location falls on the tail span, even if it lies outboard of the tip. The function of r_{vort} is to prevent singularities if this distance becomes zero. On the body, a similar relation is used:

$$VC(y) = \left(\frac{1}{r_{\text{vort}} + y_{\text{dist}}} \right)^2 (C_r)_T \tag{9}$$

Note that the use of the root chord for the area factor assumes that only the body area directly between the tail surfaces is affected. This assumption is not strictly correct, but it offers a starting point until further refinements can be made.

Using these relations, the apportionment of the wing–tail interference losses can be accomplished by summing the VC terms for both the body and tail and then taking the ratios of the summations to their combined total,

$$\left[c_{N_{T(V)}}\right]_{\text{body}} = C_{N_{T(V)}} \left[\frac{\sum_{\text{body}} VC(y)}{\sum_{\text{body}} VC(y) + \sum_{\text{tail}} VC(y)} \right] \tag{10}$$

$$\left[c_{N_{T(V)}}\right]_{\text{tail}} = C_{N_{T(V)}} \left[\frac{\sum_{\text{tail}} VC(y)}{\sum_{\text{body}} VC(y) + \sum_{\text{tail}} VC(y)} \right] \tag{11}$$

It will be assumed that the portion of the wing–tail interference load that is allocated to the body by Eq. (10) is distributed evenly along the body directly between the tail surfaces. This additional contribution is added to the total local body load at streamwise locations between the leading and trailing edges of the tail surfaces.

The portion of the wing–tail interference loads assigned to the tail surfaces by Eq. (11) is distributed across the span of the tail by assuming that its magnitude at any y location is proportional to the $VC(y)$ value [from Eq. (7)] at that location:

$$[c_n(y)]_{T(V)} = \left[C_{N_{T(V)}}\right]_{\text{tail}} \left(\frac{VC(y)}{\sum_{\text{span}} VC(y)} \right) \tag{12}$$

These loads are added to those computed in Eq. (5) to get the total local load at any spanwise location.

Changes for the Φ = 45 deg Roll Position

For the $\Phi = 45$ deg roll position, several changes must be made to the described methodology to produce a more accurate representation of the surface loads. It is obvious that there must be some way of accounting for the different aerodynamic environments experienced by the windward and leeward plane fins. In addition, the distribution of the body carryover loads induced by the lifting surfaces behave in a somewhat different fashion than for the $\Phi = 0$ deg case. The following sections describe the modifications that were made to the methodology just described to accommodate these differences.

Body–Wing and Body–Tail Interference Load Changes

The AP95 body-alone normal force is considered to be independent of roll position. However, the body–wing and body–tail interference effects will change with the roll configuration. The $\Phi = 45$ deg interference factors are computed automatically when this option is selected and are simply substituted for $\Delta C_{N_{B(W)}}$ and $\Delta C_{N_{B(T)}}$ in all computations. The values of these interference factors were chosen to give good agreement with experiment for the total loads and center of pressure. Unfortunately, when compared to CFD data, it appears that they do not produce an accurate distribution of those loads along the body or on the leeward plane tail fins. There appear to be three physical phenomena that account for these discrepancies. The first of these will be discussed now and the others in the discussions that follow.

On the surface of the body between the lifting surfaces, there is a region of high dynamic pressure. Immediately behind the lifting surfaces, however, if there is an afterbody present, there is an area where the dynamic pressure is much lower. The current AP95 methodology at $\Phi = 45$ deg averages this difference out to get the right total normal force and adds a center of pressure shift, which accounts for the inconsistencies in distribution. If the distribution of the body carryover loads is to be modeled correctly, some consideration must be given to the physics of the problem. What appears to be happening, based on the experimental data,[1] is that, in the region of the lifting surfaces, there is an enhancement to the body load at both the $\Phi = 0$ and 45 deg roll positions. At $\Phi = 0$ deg, this enhancement can extend several body diameters downstream into the traditional Mach line influence region. The method employed to model this effect was discussed earlier in this paper. At $\Phi = 45$ deg, the body loads are also strongly influenced in the immediate vicinity of the lifting surfaces. Downstream of the fins, however, the high dynamic pressure appears to decrease rapidly and produce a region of overexpansion where the body carryover actually becomes negative and total loads fall below those of the body alone. Thus, with an afterbody present, the body carryover load is lower than with no afterbody. (Note that the reverse is true at the $\Phi = 0$ deg roll orientation.)

Reference 2 models this effect with a lower minimum value of $K_{B(W)}$ at $\Phi = 45$ deg vs $\Phi = 0$ deg and a forward shift of the center of pressure. This approach, however, does not produce the proper distribution of the interference loads. For the present work, the following technique was used to partially accomplish the goal of accurate interference load distribution at $\Phi = 45$ deg. It is first assumed that, for the purpose of computing the body carryover load distribution, the minimum value of $K_{B(W)}$ is the same at $\Phi = 45$ deg as it is at $\Phi = 0$ deg. This value of $[K_{B(W)}]_{\min}$ is distributed in the vicinity of the lifting surfaces for both roll orientations as described for $\Phi = 0$ deg roll. However, for the $\Phi = 45$ deg roll position, an amount equal to

$$\Delta K_{B(W)} = \left\{\left[K_{B(W)}\right]_{\min}\right\}_{\Phi=0} - \left\{\left[K_{B(W)}\right]_{\min}\right\}_{\Phi=45} \tag{13}$$

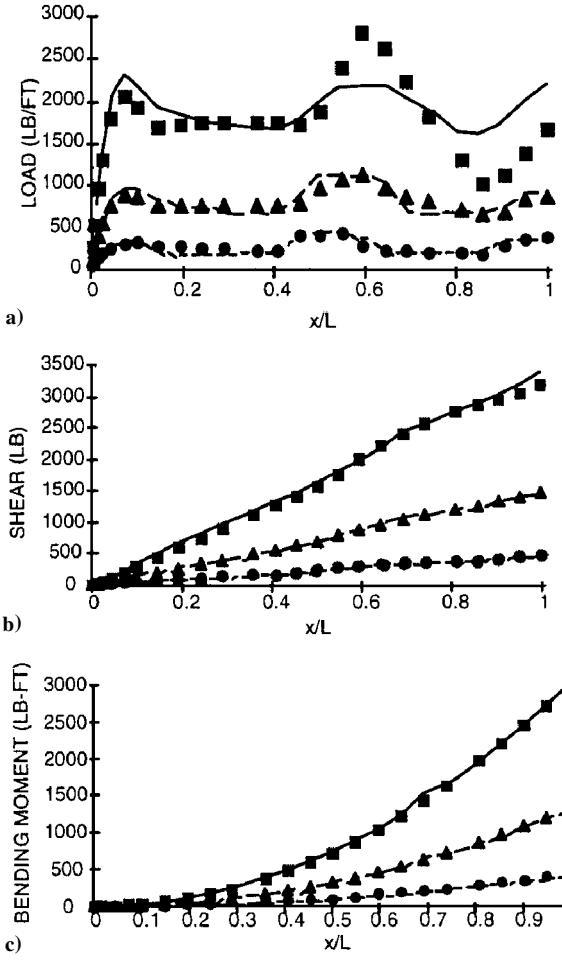

Fig. 2 Body load, shear, and bending moment: Φ = 0 deg and α = 40 deg: ——, M = 4.60, AP; ■, M = 4.60, CFD; — –, M = 2.87, AP; ▲, M = 2.87, CFD; — - -, M = 1.50, AP; and ●, M = 1.50, CFD.

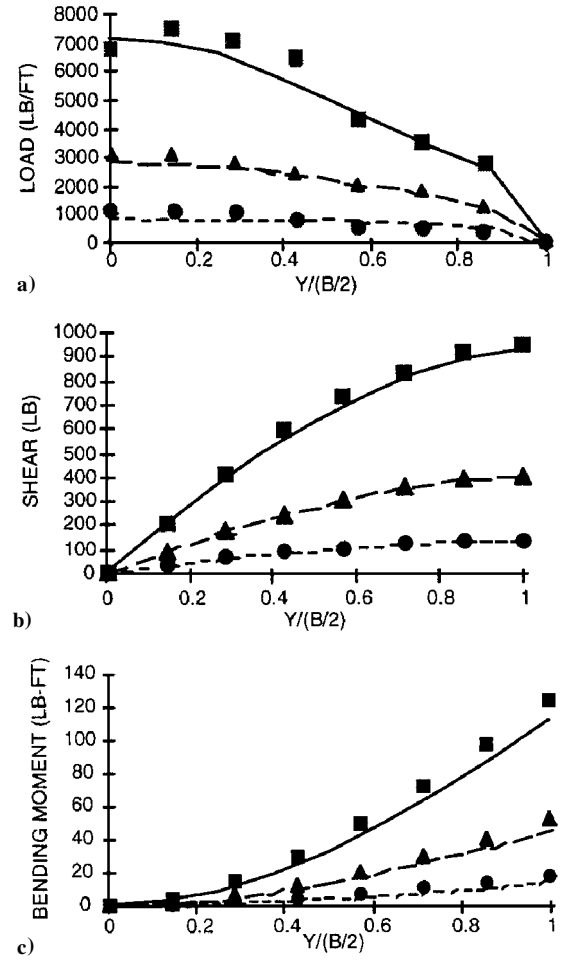

Fig. 3 Wing load, shear, and bending moment: Φ = 0 deg and α = 40 deg: ——, M = 4.60, AP; ■, M = 4.60, CFD; — –, M = 2.87, AP; ▲, M = 2.87, CFD; — - -, M = 1.50, AP; and ●, M = 1.50, CFD.

is subtracted from $K_{B(W)}$ in the region downstream of the fins. The reader is once again referred to Ref. 5 for the details of how this is done.

Lifting Surface Load Changes

When a missile is rolled into the cross (×) ($\Phi = 45$ deg) position, the lower (windward plane) and upper (leeward plane) lifting surfaces will experience different aerodynamic environments. The normal force computed by the AP95 code is the total for all fins, both windward and leeward, and it must be divided between the two planes. To accomplish this division, the approach previously used in Ref. 2 is employed. It is assumed, in agreement with slender body theory, that at an AOA of zero the normal force is evenly distributed between the windward and leeward planes. As the AOA is increased, the load on the windward surfaces is increased linearly up to 90% of the total at $\alpha = 65$ deg. This percentage remains constant up to $\alpha = 90$ deg. On the other hand, the load on the leeward plane decreases in a corresponding fashion so that the total of the two is not changed. Thus, we have at $\alpha \leq 65$ deg

$$[c_n(y)]_{\text{windward}} = [c_n(y)][0.5 + 0.4(\alpha/65)] \tag{14}$$

$$[c_n(y)]_{\text{leeward}} = [c_n(y)][0.5 - 0.4(\alpha/65)] \tag{15}$$

and at $\alpha > 65$ deg

$$[c_n(y)]_{\text{windward}} = 0.9[c_n(y)] \tag{16}$$

$$[c_n(y)]_{\text{leeward}} = 0.1[c_n(y)] \tag{17}$$

A further point to consider is that the normal forces that are computed by the AP95 code are normal only to horizontal lifting surfaces in the $\Phi = 0$ deg roll orientation. In the $\Phi = 45$ deg case, the loads given by Eqs. (14–17) must be divided by cos Φ on the windward side and by sin Φ on the leeward side to relate them to structural loads that are normal to the surfaces.

The portion of the wing–tail interference $C_{N_{T(V)}}$ that is allocated to the tail surfaces must also be divided between the windward and leeward planes. Once again relying on methodology developed in Ref. 2, this division is accomplished using the wing–tail interference factors defined during the modified slender body derivation of this term. The mathematics of this process are quite involved and will not be repeated here. For more information, the reader may consult the cited reference. For the present purpose, if i_1 is the interference factor associated with the windward plane fin and i_4 the one with the leeward plane fin, then

$$\left[C_{N_{T(V)}}\right]_{\text{windward}} = \left[C_{N_{T(V)}}\right]_{\text{tail}} \left(\frac{i_1}{i_1 + i_4}\right) \tag{18}$$

and

$$\left[C_{N_{T(V)}}\right]_{\text{leeward}} = \left[C_{N_{T(V)}}\right]_{\text{tail}} \left(\frac{i_4}{i_1 + i_4}\right) \tag{19}$$

This brings us to the second physical phenomenon, which is not explicitly modeled in the approach just outlined. In the $\Phi = 45$ deg roll position, there is a shadowing effect on the leeward plane lifting surfaces for high Mach number flows. A shadowed region exists near the root chord where Newtonian theory predicts a pressure coefficient of zero. As a result, the predicted values of loads on the leeward plane lifting surfaces, to be presented later, will be high, but due to the complexities involved in trying to model this effect, no

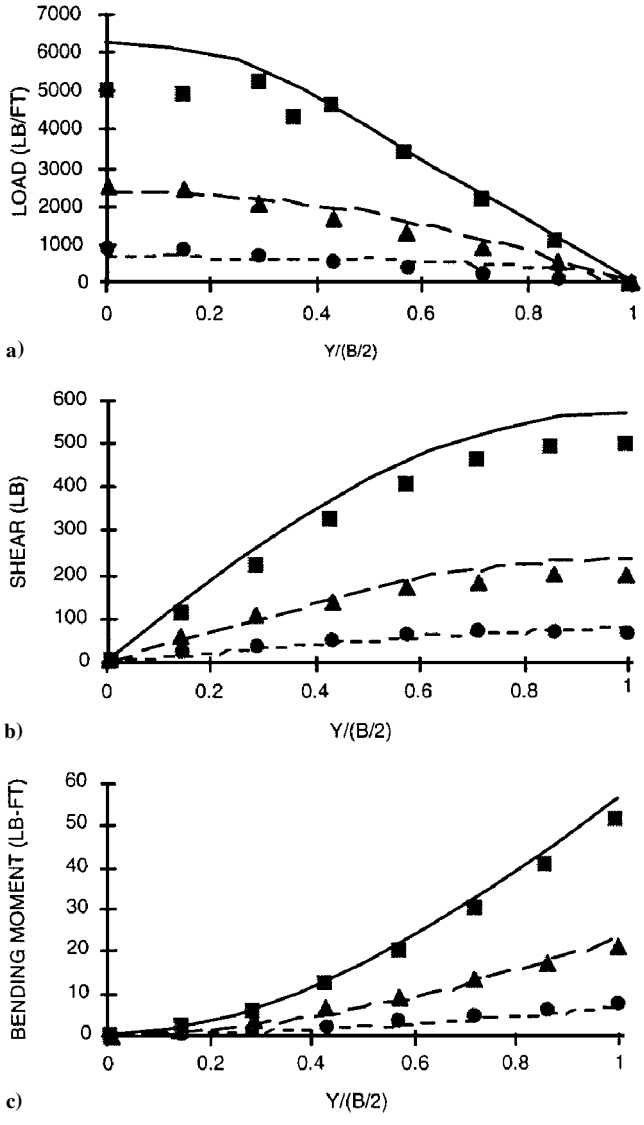

Fig. 4 Tail load, shear, and bending moment: $\Phi = 0$ deg and $\alpha = 40$ deg: ——, $M = 4.60$, AP; ■, $M = 4.60$, CFD; — –, $M = 2.87$, AP; ▲, $M = 2.87$, CFD; — - -, $M = 1.50$, AP; and ●, $M = 1.50$, CFD.

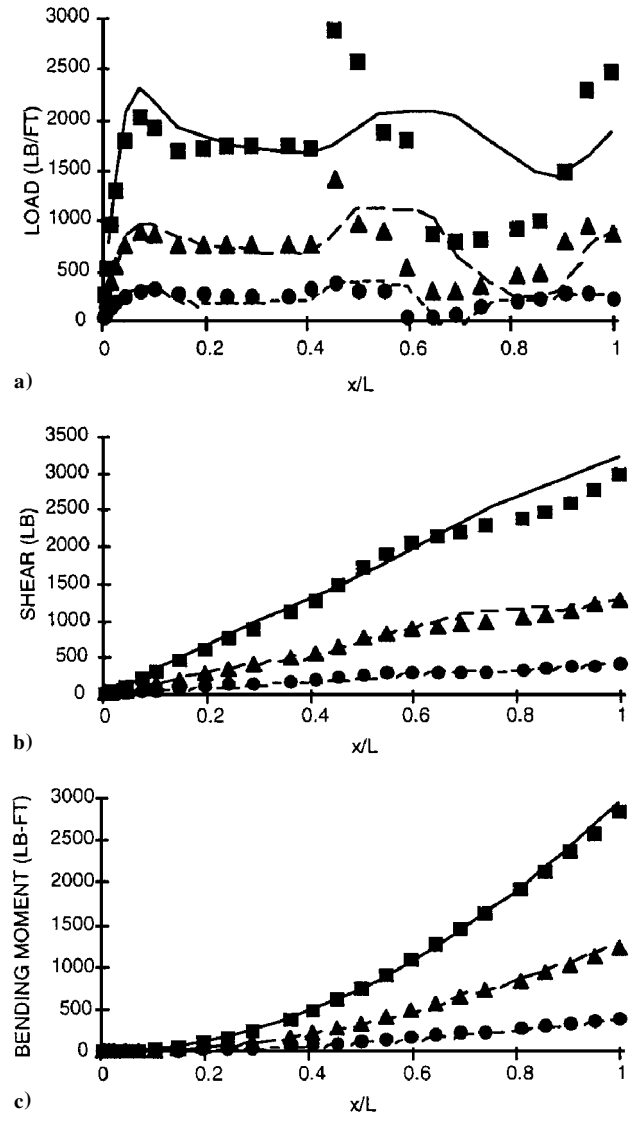

Fig. 5 Body load, shear, and bending moment: $\Phi = 45$ deg and $\alpha = 40$ deg: ——, $M = 4.60$, AP; ■, $M = 4.60$, CFD; — –, $M = 2.87$, AP; ▲, $M = 2.87$, CFD; — - -, $M = 1.50$, AP; and ●, $M = 1.50$, CFD.

attempt has been made to do so at this time. The higher the Mach number, the more accurate the Newtonian prediction of zero pressure coefficient in the shadowed region becomes. This, therefore, means that the current leeward plane loads near the body will become less accurate as Mach number increases.

The final phenomenon, which is believed to affect the load distributions but is not yet fully modeled, involves the stronger influence of body vortices on the leeward plane fins as their location is moved farther aft on the body. In the development of the semiempirical approach of the AP95, the body vortex effects were inherently included in the body carryover load. Hence, the body carryover load was lower for the tail fins than it should have been to offset the fact that the vortices actually cause the leeward plane tail fins to lose more normal force the farther aft they are located. To account for this, negative contributions from the adjusted body-lifting surface interference loads that cannot be distributed on the afterbody due to lack of sufficient length will be carried over to the leeward plane tail fins. They will be distributed along the span in the same manner as the linear and nonlinear lifting surface loads.

Loads, Shear, and Bending Moments

The primary purpose of computing load distributions over the components of a missile body is to allow the determination of shear and bending moment within the structural members. The loads that have been determined so far are nondimensional in the sense that they represent a normal force coefficient per unit length. Multiplying them by the dynamic pressure and the reference area will give local loads in pounds per foot. These loads can be integrated to get the local shear in pounds and the shear can in turn be integrated to get the local moment in pound-feet. For the body, utilizing the results of the theoretical discussions, we have for the dimensionalized local loads $w(x)$

$$w(x)_b = \left[\left(c_{n_B}\right)_L + \left(c_{n_B}\right)_{NL_{\text{adj}}} + \Delta c_{n_{B(W)}} + \Delta c_{n_{B(T)}} + \left(c_{n_B}\right)_{T(V)}\right] Q A_{\text{ref}} \tag{20}$$

We can then integrate to get the shear $V(x)_B$ and the bending moment $BM(x)_B$:

$$V(x)_B = \int_0^x w(x)_B \, dx \tag{21}$$

$$BM(x)_B = \int_0^x V(x)_B \, dx \tag{22}$$

The procedure for the lifting surfaces is the same except for the spanwise rather than the streamwise variation of the loads. For the wing, using the nondimensional load from Eq. (4), we get

$$w(y)_W = \{[c_n(y)]_W\} Q A_{\text{ref}} \tag{23}$$

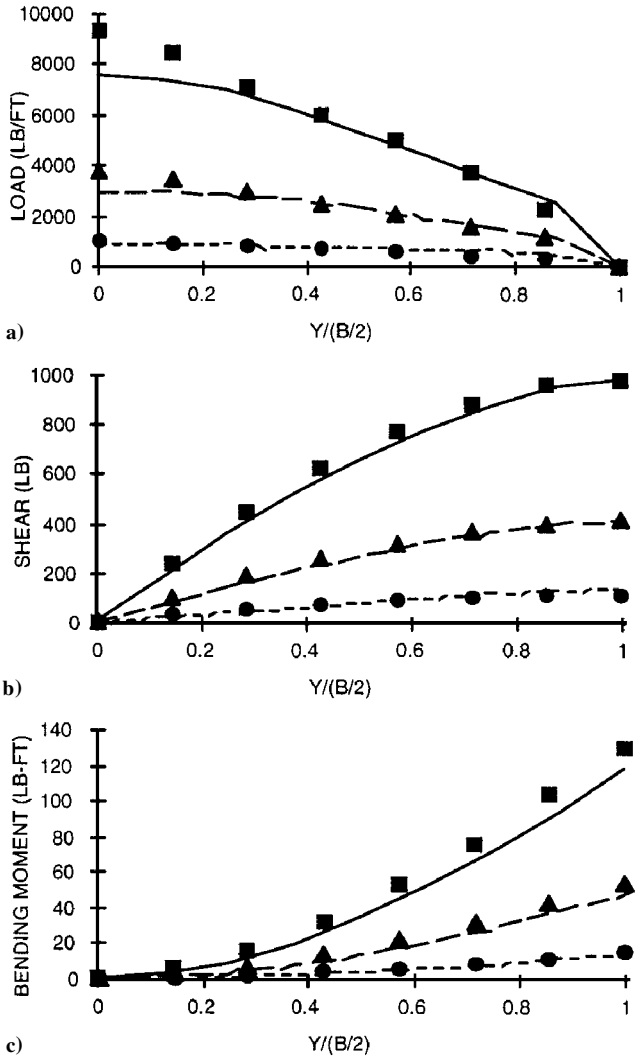

Fig. 6 Windward wing load, shear, and bending moment: Φ = 45 deg and α = 40 deg: ——, M = 4.60, AP; ■, M = 4.60, CFD; — –, M = 2.87, AP; ▲, M = 2.87, CFD; — - -, M = 1.50, AP; and ●, M = 1.50, CFD.

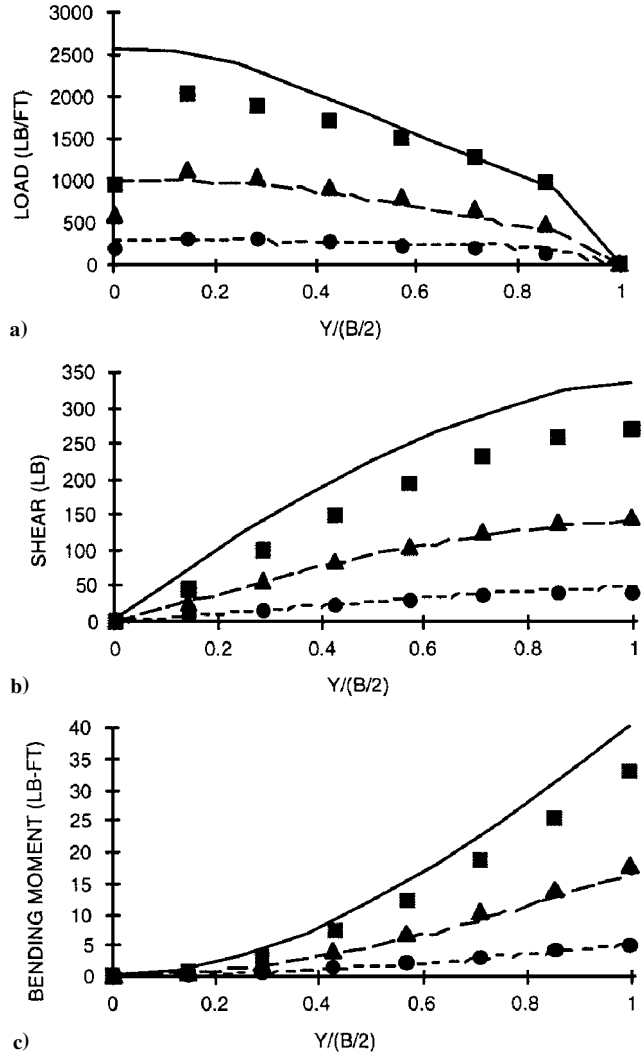

Fig. 7 Leeward wing load, shear, and bending moment: Φ = 45 deg and α = 40 deg: ——, M = 4.60, AP; ■, M = 4.60, CFD; — –, M = 2.87, AP; ▲, M = 2.87, CFD; — - -, M = 1.50, AP; and ●, M = 1.50, CFD.

For the tail, there may be a contribution from the wing–tail interference in addition to the nondimensional load from Eq. (5). That is,

$$w(y)_T = \{[c_n(y)]_T + [c_n(y)]_{T(V)}\} Q A_{\text{ref}} \tag{24}$$

Equations (23) and (24), as just presented, are valid for the $\Phi = 0$ deg roll position. For the $\Phi = 45$ deg case, there will be separate loads for the windward and leeward sets of lifting surfaces. These separate loads can be computed simply by substituting the windward and leeward values of the $[c_n(y)]_W$, $[c_n(y)]_T$, and $[c_n(y)]_{T(V)}$ contributions into Eqs. (23) and (24). The integration for shear and bending moment will be the same for both lifting surfaces and for both roll orientations. With the W/T subscript indicating the appropriate value for either the wing or tail, we have

$$V(y)_{W/T} = \int_0^y w(y)_{W/T}\, \mathrm{d}y \tag{25}$$

$$BM(y)_{W/T} = \int_0^y V(y)_{W/T}\, \mathrm{d}y \tag{26}$$

All of the preceding integrations are performed in the AP95 code using the trapezoidal rule.

Results and Discussion

For purposes of validation, the results computed by the new Aeroprediction (AP) methodology are compared to thin layer NS[4] computer calculations performed by Housh at the Naval Air Warfare Center, Weapons Division. Distributions of aerodynamic loads, shear, and bending moment were generated[5] by both methods for the wing–body–tail missile configuration of Fig. 1 at Mach numbers of 1.50, 2.87, and 4.60 and AOAs of 10, 25, and 40 deg. The configuration shown in Fig. 1, with its two sets of lifting surfaces, provides an opportunity to exercise all of the new additions to the code. The results of these computations are presented and discussed in the following. The general format followed is to handle each component (body, wing, tail) separately. Each figure has the local load, shear, and bending moment for each missile component. In all cases, CFD results are plotted together with the AP results for comparison purposes. Because of the number of figures given in Ref. 5, only the highest AOA case (AOA = 40 deg) will be presented. This case illustrates some of the more extreme shock interaction results and is the worst case for comparison of the AP results with the CFD in terms of accuracy of loads. The other AOA and additional cases are given in Ref. 5.

Figures 2–4 give the $\Phi = 0$ deg roll results for the body, wing, and tail, respectively. Figures 2a, 3a, and 4a give the local load; Figs. 2b, 3b, and 4b give the shear; and Figs. 2c, 3c, and 4c give the bending moments. In general, the AP results compared to the CFD results are very good for the body, wing, and bending moment. This is especially impressive in light of the fact that the aeroprediction code is semiempirical and the CFD is a thin-layer NS code. The areas of disagreement are primarily on the body load in the nose region and in the vicinity of the wing where the AP results are slightly high in the nose region (Fig. 2a) and the interference results tend to be smeared out in the vicinity of the wing. On average, however, when the loads are integrated, excellent results are obtained for shear and

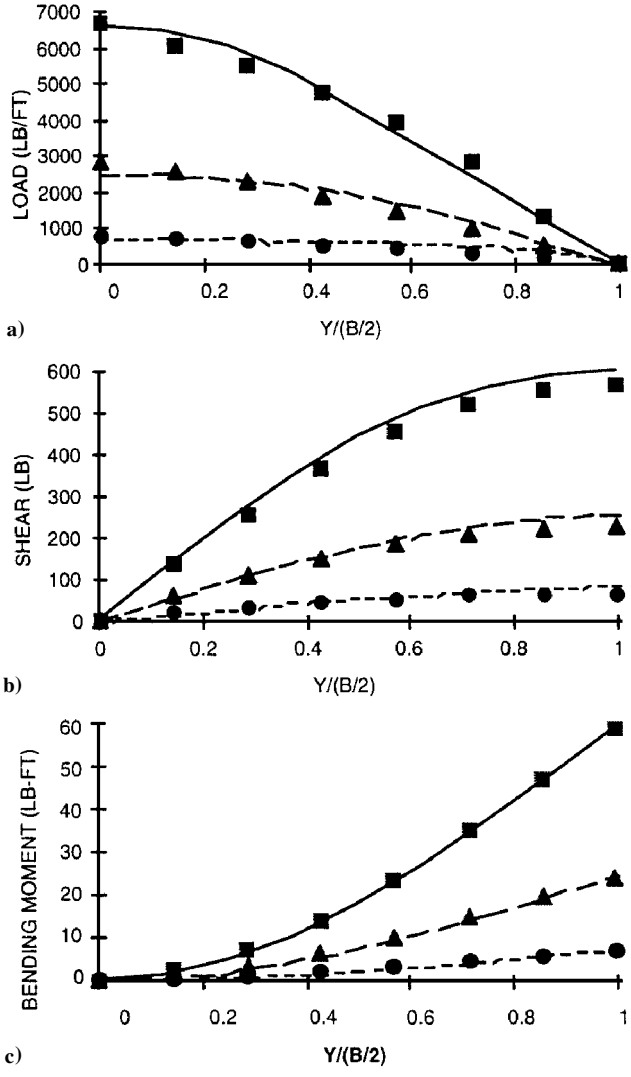

Fig. 8 Windward tail load, shear, and bending moment: Φ = 45 deg and α = 40 deg: ——, M = 4.60, AP; ■, M = 4.60, CFD; — –, M = 2.87, AP; ▲, M = 2.87, CFD; — - -, M = 1.50, AP; and ●, M = 1.50, CFD.

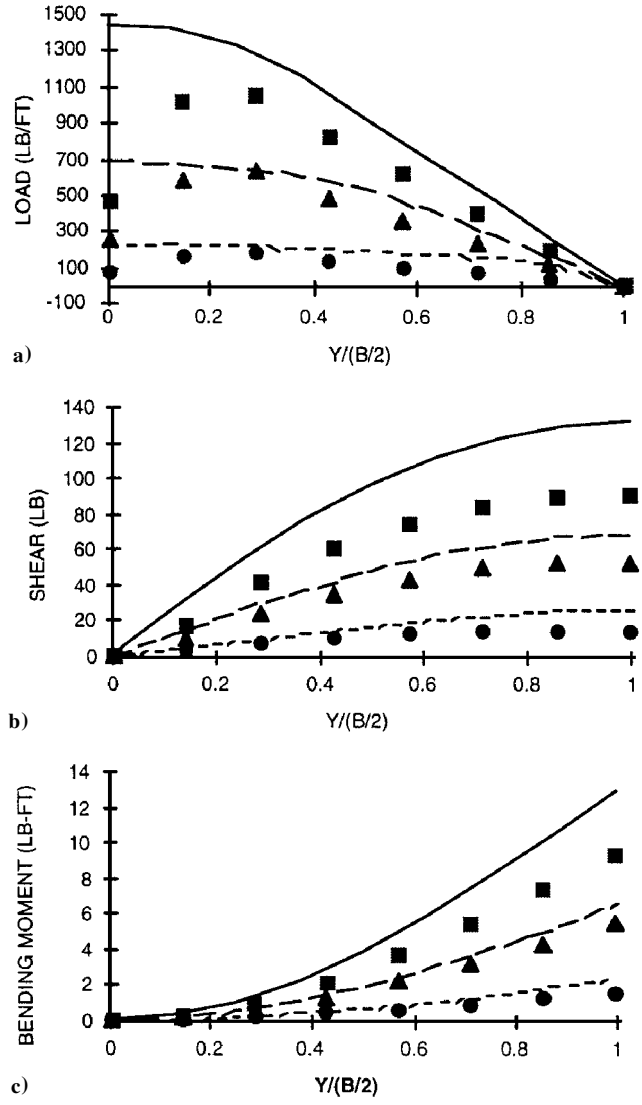

Fig. 9 Leeward tail load, shear, and bending moment: Φ = 45 deg and α = 40 deg: ——, M = 4.60, AP; ■, M = 4.60, CFD; — –, M = 2.87, AP; ▲, M = 2.87, CFD; — - -, M = 1.50, AP; and ●, M = 1.50, CFD.

bending moment. The only area of disagreement on the wing and tail is the load near the wing root at the higher Mach number. Once again, when the loads are integrated, shear and bending moment comparisons to the CFD results, in general, are very good.

Figures 5–9 give the $\Phi = 45$ deg roll results. Here the figures follow the same pattern as for Figs. 2–4 except both the windward and leeward plane wing and tail results are shown. Once again, the reader is reminded that these results are normal to the lifting surfaces or body. This means that to compare shear and bending moments to the aerodynamic normal force and pitching moments, results for the windward and leeward fins must be added and multiplied by 0.707.

Note for the $\Phi = 45$ deg body load, the CFD predictions show a sharp rise for the body loads in the vicinity of the wings followed by a rapid decrease below body-alone values behind the wings. This behavior is only partially captured in the AP results, which show a smoother rise with a lower peak and a lesser decline behind the wings. As already discussed, modifications were made to the body carryover methodology for the $\Phi = 45$ deg roll position to improve the modeling of this phenomenon. These changes have resulted in an improvement in the code's performance in this region, but the sharp surface pressure variations are still not completely modeled. The physical mechanism that gives rise to the pressure spike and the following overexpansion is not completely understood at the present time and, because it is most likely associated with strong shock interactions on the surface, it is considered beyond the scope of the present work to try and develop a more rigorous model. Figures 5b and 5c show the results for the shear force and bending moment distributions. The agreement with the CFD results is quite good, especially considering the body load variations.

The spanwise load distributions for the windward plane wings are plotted in Fig. 6a. The agreement between the AP and CFD results is very good with only some minor deviations at $M = 4.60$. The shear loads are shown in Fig. 6b. Again, the agreement is quite good between the two methods. The bending moments, presented in Fig. 6c, show a general tendency to be slightly low relative to the CFD results but overall agreement is good.

The load distributions for the leeward wings are shown in Fig. 7a. It can be seen that the shadowing effect discussed in the "Lifting Surface Load Changes" section is quite evident for the $M = 2.87$ and 4.60 cases. The CFD results predict a large pressure loss on the wings in the shadowed region near the body, which is not modeled in the AP code. Otherwise, agreement is very good. The shear distributions are shown in Fig. 7b, and, as might be expected, there is significant overprediction at the higher Mach numbers relative to the CFD results, but the results are still surprisingly good. The same comments apply to the bending moments, which are presented in Fig. 7c.

Figure 8 shows the windward tail loads, shear, and bending moment. The agreement between the two approaches is quite good.

The leeward tail loads are plotted in Fig. 9a. As for the leeward wings, the shadowing effect is very obvious at the two higher Mach numbers. The shear loads, shown in Fig. 9b, and the bending moments, shown in Fig. 9c, are overpredicted relative to the CFD results

because of this effect. Note that, by modifying the body carryover prediction methodology for the $\Phi = 45$ deg case and applying any excess negative contributions to the leeward tail, the results for the leeward tail have been improved substantially over their original values. However, because of the complex nature of leeside flowfields at high AOAs, it is extremely difficult to develop empirical models that will give truly accurate results in these regions.

Summary

New methodology has been added to the Naval Surface Warfare Center, Dahlgren Division, AP code to compute both the linear and nonlinear contributions to surface loads and to distribute these loads over the body and lifting surfaces. The new methods include models to simulate lifting surface interference effects on the body for both the $\Phi = 0$ and 45 deg roll positions. At $\Phi = 45$ deg, load distributions are computed for both the windward and leeward lifting surfaces. Wing–tail interference loads are now separated into components, which are distributed along the body in the vicinity of the tail as well as across the tail surfaces themselves. All loads are integrated to give shear and bending moment distributions, which may be used by structural engineers in the design process.

As an aid in developing the new techniques, and for validation purposes, results from NS CFD computations for a wing–body–tail missile configuration were utilized after the CFD results had been validated against experimental data. In general, the AP methodology proved to be quite successful at modeling the distribution of surface loads when compared to the CFD results. The only exceptions occurred for the $\Phi = 45$ deg roll position where the loads on leeside lifting surfaces (especially tail surfaces) tended to be overpredicted and the exaggerated pressure variations on the body in the vicinity of lifting surfaces were not fully captured.

With these new additions, the AP code should prove to be a much more useful tool to the structural engineer who is interested in performing preliminary structural analyses of several competing missile designs. To the authors' knowledge, it will be the only semiempirical aerodynamics code available with this capability.

Acknowledgments

The work described in this paper was supported through the Office of Naval Research (Dave Siegel) by the following programs: the Air Launched Weapons Program managed at the Naval Air Warfare Center, China Lake, California, by Tom Loftus and Craig Porter and the Surface Weapons Systems Technology Program managed at the Naval Surface Warfare Center, Dahlgren Division (NSWCDD), by Robin Staton and Gil Graff. Also, some support was provided by the Marine Corps Weaponry Technology Program managed at NSWCDD by Bob Stiegler. The authors express appreciation for support received in this work.

References

[1]Moore, F. G., McInville, R. M., and Hymer, T. C., "The 1995 Version of the NSWC Aeroprediction Code: Part I—Summary of New Theoretical Methodology," U.S. Naval Surface Warfare Center, Dahlgren Div., Rept. NSWCDD/TR-94/379, Dahlgren, VA, Feb. 1995.

[2]Moore, F. G., and McInville, R. M., "Extension of the NSWCDD Aeroprediction Code to the Roll Position of 45 Degrees," U.S. Naval Surface Warfare Center, Dahlgren Div., Rept. NSWCDD/TR-95/160, Dahlgren, VA, Dec. 1995.

[3]Monta, W. J., "Supersonic Aerodynamic Characteristics of a Sparrow III Type Missile Model with Wing Controls and Comparison with Existing Tail-Control Results," NASA TP 1078, Oct. 1977.

[4]Buning, P. G., et al., "Overflow User's Manual," Version 1.6an, June 1995.

[5]McInville, R. M., Moore, F. G., and Housh, C., "Nonlinear Structural Load Distribution Methodology for the Aeroprediction Code," U.S. Naval Surface Warfare Center, Dahlgren Div., Rept. NSWCDD/TR-96/133, Dahlgren, VA, Sept. 1996.

[6]Moore, F. G., "Body Alone Aerodynamics of Guided and Unguided Projectiles at Subsonic, Transonic, and Supersonic Mach Numbers," U.S. Naval Surface Warfare Center, Dahlgren Div., Rept. NWL TR-2796, Dahlgren, VA, Nov. 1972.

[7]Moore, F. G., Armistead, M. A., Rowles, S. H., and De Jarnette, F. R., "Second-Order Shock-Expansion Theory Extended to Include Real Gas Effects," U.S. Naval Surface Warfare Center, Dahlgren Div., Rept. NAVSWC TR 90-683, Dahlgren, VA, Feb. 1992.

[8]Moore, F. G., and McInville, R. M., "A New Method for Calculating Wing Alone Aerodynamics to Angle of Attack 180°," U.S. Naval Surface Warfare Center, Dahlgren Div., Rept. NSWCDD/TR-94/3, Dahlgren, VA, March 1994.

[9]Stallings, R. L., and Lamb, M., "Wing Alone Aerodynamic Characteristics for High Angles of Attack at Supersonic Speeds," NASA TP 1889, July 1981.

[10]Baker, W. B., Jr., "Static Aerodynamic Characteristics of Generalized Slender Bodies With and Without Fins at Mach Numbers from 0.6 to 3.0 and Angles of Attack from 0 to 180°," Arnold Engineering Development Center, Rept. AEDC-TR-75-124, Vols. 1 and 2, Tullahoma, TN, May 1976.

[11]Nielsen, J. N., Hemsch, M. J., and Smith, C. A., "A Preliminary Method for Calculating the Aerodynamic Characteristics of Cruciform Missiles to High Angles of Attack Including Effects of Roll Angle and Control Deflections," Office of Naval Research, Rept. ONR-CR215-226-4F, Arlington, VA, Nov. 1977.

R. M. Cummings
Associate Editor